



HAL
open science

Double Stimuli-Responsive Perforated Lamellar Structure Formed by Linear ABC Triblock Terpolymer Monoliths

Hana Bouzit, Felix Krusch, Daniel Hermida-Merino, Eduardo Solano, Didier Cot, J.P. Mericq, Stéphanie Roualdes, Mona Semsarilar, Damien Quemener, Karim Aissou

► **To cite this version:**

Hana Bouzit, Felix Krusch, Daniel Hermida-Merino, Eduardo Solano, Didier Cot, et al.. Double Stimuli-Responsive Perforated Lamellar Structure Formed by Linear ABC Triblock Terpolymer Monoliths. *Journal of Polymer Science*, 2022, 10.1002/pol.20220264 . hal-03715575

HAL Id: hal-03715575

<https://hal.science/hal-03715575>

Submitted on 6 Jul 2022

HAL is a multi-disciplinary open access archive for the deposit and dissemination of scientific research documents, whether they are published or not. The documents may come from teaching and research institutions in France or abroad, or from public or private research centers.

L'archive ouverte pluridisciplinaire **HAL**, est destinée au dépôt et à la diffusion de documents scientifiques de niveau recherche, publiés ou non, émanant des établissements d'enseignement et de recherche français ou étrangers, des laboratoires publics ou privés.

Double Stimuli-Responsive Perforated Lamellar Structure Formed by Linear ABC Triblock Terpolymer Monoliths

Hana Bouzit,¹ Felix, Krusch,¹ Daniel Hermida-Merino,^{2,3} Eduardo Solano,⁴ Didier Cot,¹ Jean Pierre Méricq,¹ Stéphanie Roualdes,¹ Mona Semsarilar,¹ Damien Quémener,¹ and Karim Aissou^{1*}

¹Institut Européen des Membranes, IEM, UMR 5635, Univ Montpellier, ENSCM, CNRS, Montpellier, France

²DUBBLE CRG BM26@ESRF, Netherlands Organization for Scientific Research (NWO), 71 Avenue des Martyrs, 38000 Grenoble, France

³Departamento de Física Aplicada, CINBIO, Universidade de Vigo, Campus Lagoas-Marcosende, E36310 Vigo, Galicia, Spain

⁴ALBA Synchrotron Light Source, NCD-SWEET Beamline, Cerdanyola del Valles, 08290 Spain

E-mail: karim.aissou@umontpellier.fr

Abstract: Amphiphilic block copolymer (BCP) thick films with stimuli-responsive pores are promising candidates for the manufacturing of next-generation ultrafiltration (UF) membranes since their smart nanochannels facilitates the removal of fouling which is considered as one of the biggest challenges in membrane technology. In this work, a well-defined polystyrene-*block*-poly(2-vinylpyridine)-*block*-poly(*N*-isopropylacrylamide) (PS-*b*-P2VP-*b*-PNIPAM) terpolymer was prepared for the first time *via* reversible addition-fragmentation chain transfer (RAFT) polymerization. The combination of the nonsolvent-induced phase separation (NIPS) process with a solvent vapor annealing (SVA) treatment was used to produce nanostructured pH- and thermo-double sensitive ABC-type BCP thick films. Here, the NIPS-made PS-*b*-P2VP-*b*-PNIPAM thick film, comprising a microporous spinodal-type network substructure, topped by a dense thin layer of poorly defined nanopores is transformed into a monolith entirely composed of a well-ordered perforated lamellar (PL) phase upon exposure to a chloroform vapor during 6h. Such kind of PL-structured monoliths, showing a permeance value as high as 18 L.h⁻¹.m⁻².bar⁻¹ at 46°C and pH = 7 with an excellent temperature cyclability, are highly desired to manufacture smart separation-based UF materials able to transit their pore state from hydrophilic to hydrophobic (and vice versa), thereby leading to much more efficient detachment of foulants during the cleaning process.

Keywords: PS-*b*-P2VP-*b*-PNIPAM, RAFT polymerization, thermo-sensitive, pH-responsive, membrane.

Introduction

Over the last decade, amphiphilic block copolymers (BCPs) have attracted extensive attention to manufacture ideal membranes combining high selectivity and good permeability for valuable ultrafiltration (UF) applications (*e.g.*, water purification with complete rejection of virus, biopharmaceutical separations, etc.).¹⁻⁵ Such innovative materials with a better figure of merit compared to the state of the art membrane are based on the BCP self-assembly into well-ordered nanostructures leading to the formation of monodisperse pores in high areal density (up to 10 terapore per inch²) on the membrane top surface.⁶

However, in UF processes, the inevitable flux decline of membranes caused by the accumulation of foulants in the nanopores is particularly challenging to solve since low shear forces can be achieved in such small pores.⁷ One appealing approach to prevent the fouling effects (*i.e.*, flux decline, high-energy consumption and material lifetime decreasing) is the nanodesign of smart membranes with an adjustable pore shape that can be controlled by external stimuli such as temperature, pH, ion concentration and redox potential.⁸⁻¹¹ In this way, one key feature of BCP membranes is the facile implementation of specific properties within the material since microphase-separated domains afford to overcome the dilemma between the mechanical strength of the material and a macromolecular dynamic under an external stimulus required for facilitating the cleaning process.

Following this strategy, several BCP membranes containing a stimuli-responsive block have been demonstrated by using a nonsolvent-induced phase separation (NIPS) preparation method.¹²⁻¹⁶ For instance, asymmetric membranes with pH-responsive pores were achieved by using polystyrene-*block*-poly(2-vinylpyridine) (PS-*b*-P2VP) chains since the swelling/shrinking switches of the weak polyelectrolyte P2VP by protonation/deprotonation lead to a closing/opening state of the nanochannels.¹⁷ In another example, thermoresponsive PS-*b*-poly(*N*-isopropylacrylamide) (PS-*b*-PNIPAM) membranes were produced due to the lower critical solution temperature (LCST) of PNIPAM occurring at 32°C.⁷ Here the effective porosity of nanochannels can be regulated according to changes in the water temperature since the PNIPAM block swells below its LCST, thus restricting the formation of large pores and vice versa. This behavior makes that an increase of the permeability by almost 400% was observed above the PNIPAM LCST. However, the formation of monodisperse PNIPAM-based nanochannels was not demonstrated for these single-responsive PS-*b*-PNIPAM membranes. More recently, original linear and star-shaped PNIPAM-*b*-poly(vinylidene fluoride) (PNIPAM-*b*-PVDF) membranes with a thermoresponsive character were produced by Algarni and coworkers.¹⁶ Although some PNIPAM-*b*-PVDF membranes revealed an interesting zig-zag

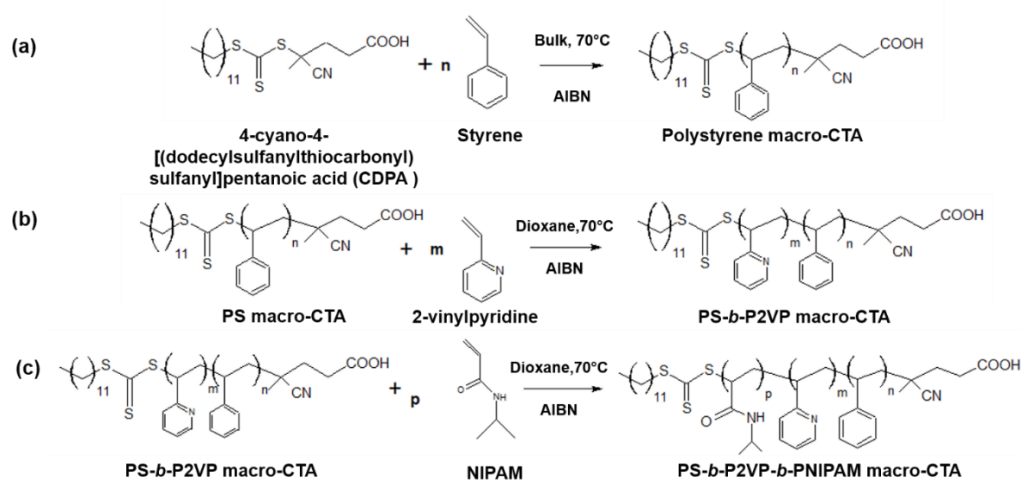
morphology at the micron scale, again monodisperse PNIPAM-based nanochannels in a high areal density were not generated during the NIPS process.

To take the concept one-step further, membranes showing both pH- and thermo-responsive behavior have also been manufactured. For instance, Clodt *et al.* have recently obtained this dual responsive behavior by coating an end-functionalized PNIPAM homopolymer on a pH-responsive PS-*b*-P4VP membrane *via* “grafting to” approach.¹⁴

Generally, in the “grafting to” approach, the diffusion of the end-functionalized homopolymers into the nanoscale pores is prevented by the polymer brushes already grafted on the membrane surface. Here, we have synthesized for the first time PS-*b*-P2VP-*b*-PNIPAM terpolymers *via* reversible addition-fragmentation chain transfer (RAFT) polymerization to produce asymmetric thick films endowed with thermo/pH dual responsive nanodomains. We show that the non-permeable NIPS-made PS-*b*-P2VP-*b*-PNIPAM thick film, consisting of a microporous (spinodal) network substructure and a dense top layer with a poorly-defined phase, is transformed into a permeable monolith entirely composed of a well-ordered perforated lamellar (PL) phase during the solvent vapor annealing (SVA) treatment. Water permeability tests were carried out to confirm the dual responsive behavior of the P2VP/PNIPAM nanopores formed within the PL-structured monolith as well as their good thermal cyclability. Such multifunctional monoliths with unique nanoscale properties provide prospect to the fabrication of efficient easy-to-clean separation based-materials.

Results and discussion

The general route used in this work to prepare PS-*b*-P2VP-*b*-PNIPAM terpolymers by RAFT polymerization is presented in **Scheme 1**.



Scheme 1. General route for RAFT polymerization of the (1) PS, (2) PS-*b*-P2VP and (3) PS-*b*-P2VP-*b*-PNIPAM macro-RAFT agents.

Our approach was to start with (1) a bulk styrene polymerization using trithiocarbonate as RAFT agent and AIBN as the initiator, (2) followed by an extension with 2VP conducted in 1,4-dioxane in presence of AIBN and (3) then with NIPAM under similar conditions. According to the literature, this RAFT polymerization approach optimizes the synthesis of the PS-*b*-P2VP-*b*-PNIPAM system since starting by a PNIPAM macroRAFT to prepare a PNIPAM-*b*-P2VP-*b*-PS terpolymer may cause retardation of the styrene polymerization due to slow initiation, slow fragmentation of the intermediate radicals and possible irreversible termination reactions.¹⁸ **Figure S1** shows the size exclusion chromatography (SEC) traces of the PS homopolymer (hPS) (purple) and PS-*b*-P2VP BCP (red) macro-RAFT agents as well as the desired PS-*b*-P2VP-*b*-PNIPAM terpolymer (green) for which the synthesis preparation conditions are detailed in the experimental section. All SEC traces exhibit a narrow, unimodal distribution with no evidence of high molecular weight polymers that may justify uncontrolled polymerization or coupling reactions. Moreover, the shift of the SEC curves toward higher molecular weights, which comes from the difference in the hydrodynamic volumes of the hPS, PS-*b*-P2VP BCP and PS-*b*-P2VP-*b*-PNIPAM terpolymer, fully supports the successful preparation of targeted ABC triblock terpolymer chains with low dispersity ($\mathcal{D} < 1.32$). Note that the molecular weight (M_n) of the hPS macroRAFT was found to be 28.2 kg/mol ($\mathcal{D} = 1.09$) using PS standards.

To determine the molecular weights of the P2VP and PNIPAM blocks, ¹H nuclear magnetic resonance (NMR) spectra of the AB- and ABC-type BCPs were used (see **Fig. S2**). By comparing the ¹H NMR integral ratios between the characteristic signal of PS at $\delta = 6.59$ -7.05 ppm and those of P2VP ($\delta = 8.25$ ppm) and PNIPAM ($\delta = 3.99$ ppm), the molar masses of the PS-*b*-P2VP and PS-*b*-P2VP-*b*-PNIPAM BCPs were calculated to be 34.6 kg/mol and 42.5 kg/mol, respectively. Therefore, the proton NMR spectroscopy indicates that PS-*b*-P2VP-*b*-PNIPAM chains consists of PS (28.2 kg/mol, $\phi_{PS} = 0.68$), P2VP (5.8 kg/mol, $\phi_{P2VP} = 0.13$) and PNIPAM (8.5 kg/mol, $\phi_{PNIPAM} = 0.19$) where ϕ represents the different volume fractions (see **Table 1**). Note that the PS-*b*-P2VP-*b*-PNIPAM chains were devised with a relatively low molecular weight in order to overcome the trade-off between the terpolymer chain mobility when exposed to a CHCl₃ vapor and sufficiently good mechanical properties to generate non-brittle (freestanding) films.

Block	PS	P2VP	PNIPAM
M_{n,NMR} (kg/mol)	28.2	5.8	8.5
Vol. fraction	0.68	0.13	0.19

Table 1: Molecular weight and composition of the PS-*b*-P2VP-*b*-PNIPAM system used in this work.

As the presence of PS homopolymer or even PS-*b*-P2VP BCP within the ABC triblock terpolymer thick film can strongly affect the phase behavior of the PS-*b*-P2VP-*b*-PNIPAM chains, the powder purity was established by 2D-diffusion-ordered spectroscopy (DOSY)-NMR (see **Fig. S3**). The NMR experiment revealed that ¹H resonances belonging to the PS, P2VP and PNIPAM blocks are aligned with the same horizontal for the PS-*b*-P2VP-*b*-PNIPAM terpolymer, thereby indicating a good purity of the powder since all the signals arise from the same macromolecule having a diffusion coefficient of $5.01 \times 10^{-11} \text{ m}^2 \cdot \text{s}^{-1}$. It is noteworthy that the diffusion coefficients of the PS and PS-*b*-P2VP chains are higher since they are found to be $6.60 \times 10^{-11} \text{ m}^2 \cdot \text{s}^{-1}$ and $8.31 \times 10^{-11} \text{ m}^2 \cdot \text{s}^{-1}$, respectively.

Thick film morphology formed by the PS-*b*-P2VP-*b*-PNIPAM terpolymer was also studied. Both the top view scanning electron microscopy (SEM) and atomic force microscopy (AFM) topographic images presented in **Figure S4** reveal the representative top surface morphology of a PS-*b*-P2VP-*b*-PNIPAM thick film that was manufactured by NIPS from a 18 wt. % polymer solution in a di-solvent mixture of 1,4-dioxane and tetrahydrofuran (DOX/THF: 1/1 w/w). These micrographs show that a dense top surface layer with poorly defined domains is produced when the mixture of di-solvents is allowed to evaporate from the PS-*b*-P2VP-*b*-PNIPAM thick film for 30s before immersing the material into a coagulation (water) bath to induce the phase inversion. To know more about the skin layer morphology and gain insight into the porosity generated by NIPS within the material, cross-sectional SEM views were also taken (see **Fig. 1**).

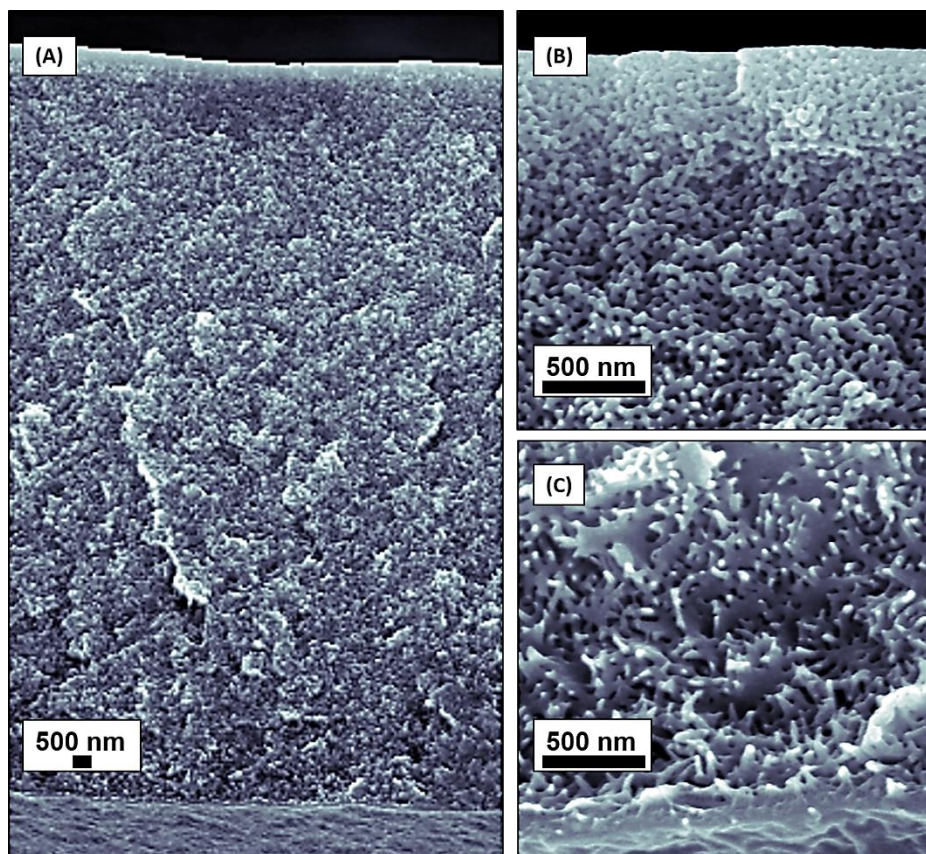


Figure 1. Cross-sectional SEM views of an asymmetric PS-*b*-P2VP-*b*-PNIPAM thick film generated by NIPS showing: (a) the full material having a thickness of $\sim 21 \mu\text{m}$, (b) a 500 nm thick top layer (light gray) with a poorly defined phase topping the sponge-like substructure, and (c) the formation of a thin dense bottom layer without any pores.

The cross-sectional SEM image of the full material reveals a $21 \mu\text{m}$ thick PS-*b*-P2VP-*b*-PNIPAM film consisting of a (dark gray) microporous spinodal-type network substructure¹⁹ and a (light gray) dense top surface layer (see **Fig. 1a**). The magnified SEM view of the upper region of the NIPS-made PS-*b*-P2VP-*b*-PNIPAM thick film confirms that the dense top layer with a thickness of $\sim 500 \text{ nm}$ exhibits a poorly defined nanophase (see **Fig. 1b**). At the opposite interface of the PS-*b*-P2VP-*b*-PNIPAM thick film, a dense thin bottom layer²⁰ (thickness of few tens of nanometers) without any open pores can be observed from the magnified SEM view taken at the vicinity of the bottom interface (see **Fig. 1c** and **S5**). The presence of a dense and non-porous surface layer at each face of the NIPS-made PS-*b*-P2VP-*b*-PNIPAM thick film should explain why the water flux across this material is zero (*i.e.*, non-permeable polymeric thick film).

One way to improve the water permeability of the PS-*b*-P2VP-*b*-PNIPAM thick films is to generate well-defined permeable nanochannels within the top and bottom dense layers. To this end, the polymeric thick films were exposed to a CHCl_3 vapor during 6h in order to promote the self-assembly of the PS-*b*-P2VP-*b*-PNIPAM chains into a thermo/pH dual responsive

nanoporous morphology. After the SVA treatment, the SEM image presented in **Figure S6** shows that the material top surface exhibits well-defined in-plane cylinders or out-of-plane lamellae arranged into large grains. The AFM topographic image presented in **Figure 2a** reveals that the equilibrium structure formed on the material top surface consists more precisely of an alternation of well-defined PS (bright) and P2VP/PNIPAM (dark) out-of-plane lamellae having a period of ~ 37 nm, as extracted from the fast Fourier transform (FFT). The associated high-resolution mapping obtained by using a Laplacian matrix deconvolution method allows distinguishing the presence of dark holes within the PS lamellae, which indicates that the nanostructure is rather a perforated lamellar (PL) phase (see **Fig. 2b**).

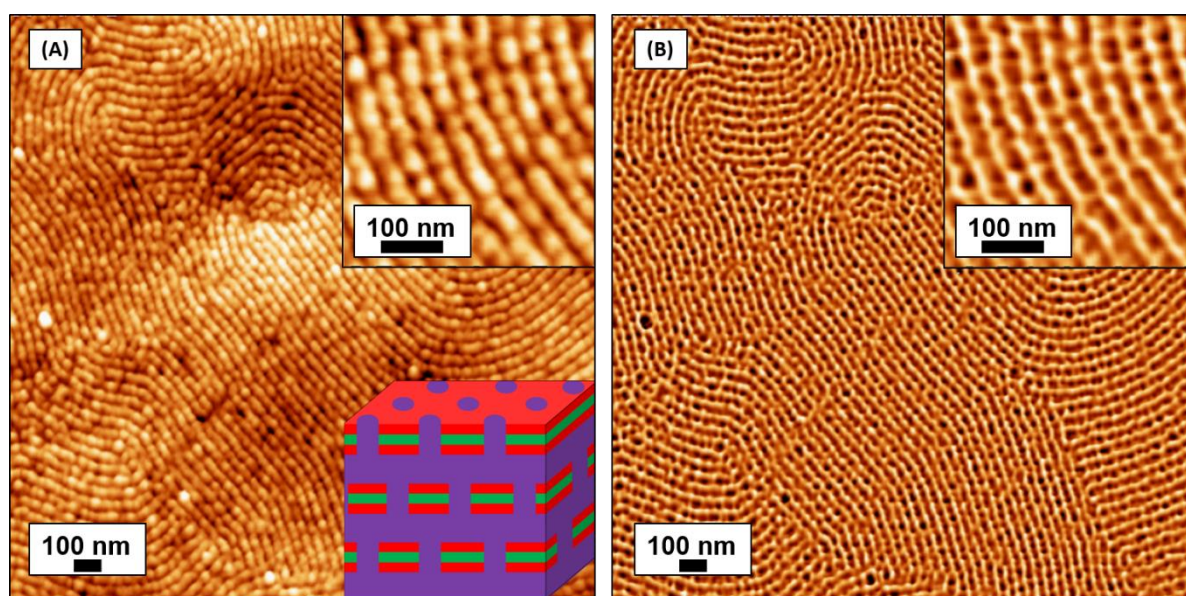


Figure 2. (a) AFM topographic view and (b) its associated high-resolution mapping obtained by using a Laplacian deconvolution matrix that show a 37 nm period fingerprint pattern formed on the top surface of a solvent-annealed (6h, CHCl_3) PS-*b*-P2VP-*b*-PNIPAM thick film subsequently treated by a CF_4 plasma. Insets: Magnified AFM topographic image and its corresponding high-resolution mapping showing the presence of lamellae with dots arising from PS perforations. Schematic representation of the PL phase showing the core-shell (green) PNIPAM-(red) P2VP lamellae perforated by (purple) PS protrusions connecting the adjacent PS lamellae.

In general, the perforation formed within the PL phase obeys either to a conventional hexagonal or tetragonal symmetry.²¹ As the symmetry of PS perforations extended through the P2VP/PNIPAM lamellae remains unclear from the AFM topographic image, grazing incidence small X-ray scattering (GISAXS) experiments were performed to elucidate the protrusion packing arrangement. The 2D GISAXS pattern presented in **Figure S7** indicates that the PS perforations are arranged into a rhombic array ($c2mm$ crystallographic group) with the lattice parameters $a = 37$ nm and $b = 26$ nm and a preferential (10) plane orientation parallel to film free surface, instead of the common hexagonal or tetragonal packings expected for a PL

structure. These results compare favorably with the cross-sectional SEM images presented in **Figure S8** showing the formation of a rhombic array with similar lattice parameters ($a = 36$ nm and $b = 26$ nm) extracted from the 2D-FFT. Note that the formation of a bicontinuous PL structure with perforations ordered into a rhombic array has been recently observed both from asymmetric poly(1,1-dimethyl silacyclobutane)-*b*-PS-*b*-P2VP thick films and their monolith homologs, depending on the SVA treatment duration.²²

Here to highlight the fabrication of monoliths entirely composed of the PL phase after the SVA treatment, cross-sectional SEM images were taken from the top, middle and bottom regions of a PS-*b*-P2VP-*b*-PNIPAM film (see **Fig. 3**). The cross-sectional SEM view presented in **Figure 3a** reveals that the PS-*b*-P2VP-*b*-PNIPAM material has densified during the SVA treatment to form a symmetric film exhibiting a well-developed PL structure (see **Figures S8 and S9**) as attested by a strong decrease of the film thickness (~ 14 μm). This phenomenon can be attributed to the growth of the nanoporous PL phase at the expense of the microporous spinodal-type network structure. Moreover, the cross-sectional images taken close to the top and bottom interfaces of the solvent-annealed (6h, CHCl_3) PS-*b*-P2VP-*b*-PNIPAM thick film show both the presence of a self-assembled structure which clearly indicates the formation of a monolith entirely composed of a nanoporous PL phase (see **Fig. 3b,c**).

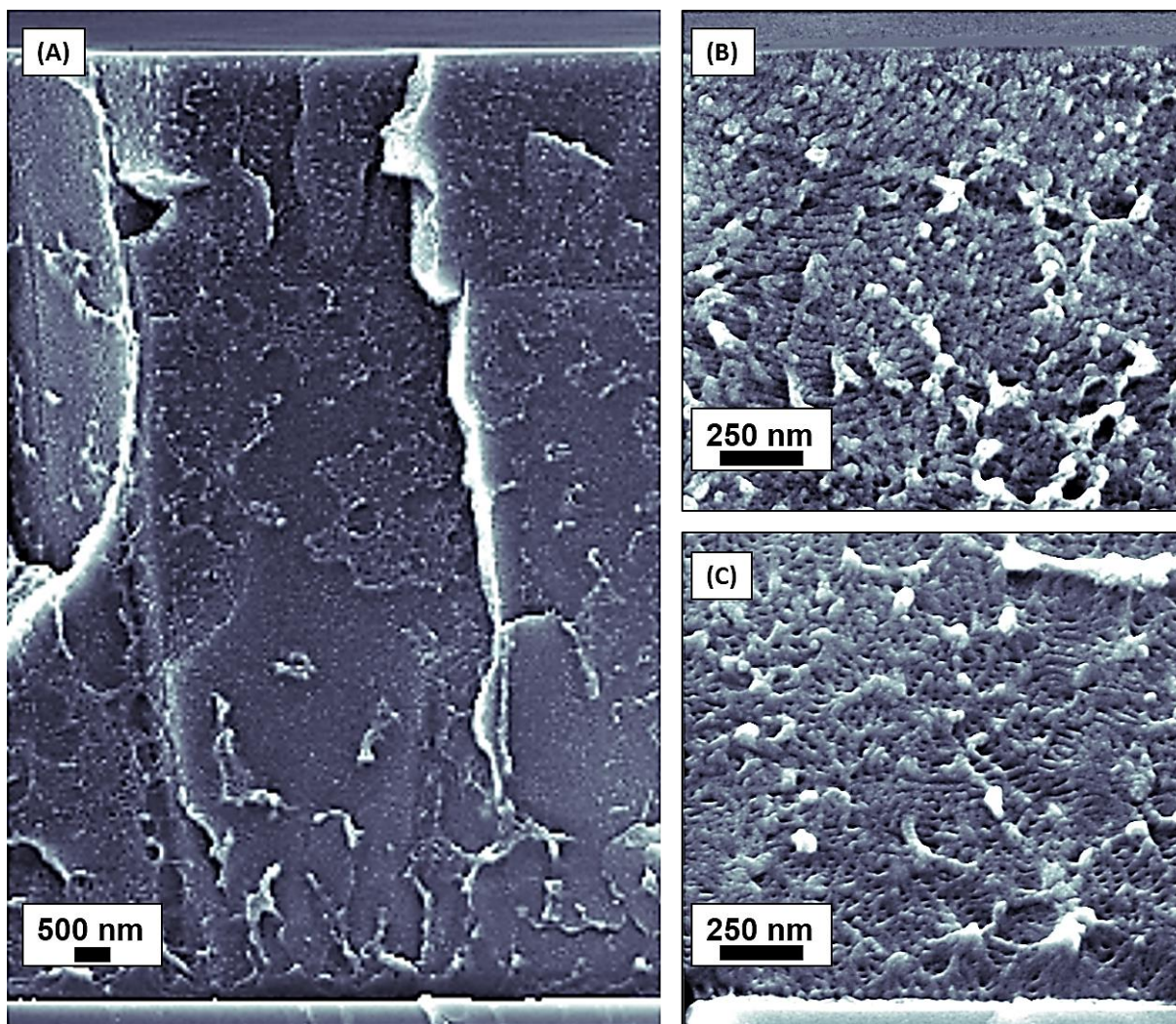


Figure 3. Cross-sectional SEM views of a solvent-annealed (6h, CHCl_3) PS-*b*-P2VP-*b*-PNIPAM thick film generated by NIPS-SVA showing (a) the full symmetric material having a thickness of $\sim 14 \mu\text{m}$ as well as the formation of the nanoporous PL phase in the vicinity of the (b) top and (c) bottom interfaces.

To show that the SVA treatment allows manufacturing PS-*b*-P2VP-*b*-PNIPAM materials endowed with thermo/pH dual responsive nanopores, flux performance tests were conducted at different water environments (*i.e.*, different temperature and pH conditions) (see **Fig. 4**). To study the thermo-responsive behavior, the water fluxes of solvent-annealed (6h, CHCl_3) PS-*b*-P2VP-*b*-PNIPAM monoliths were recorded at temperatures well below and above the LCST transition of the PNIPAM block ($\sim 32^\circ\text{C}$) under neutral pH conditions ($\text{pH} = 7$) (see **Fig. 4a**). Prior to do the measurement, the PS-*b*-P2VP-*b*-PNIPAM monoliths generated by NIPS-SVA were deposited on a highly permeable polyvinylidene difluoride (PVDF) support and the permeance was then plotted as the function of the water pressure applied from 0.5 to 2 bar, using a dead-end stirred ultrafiltration cell.²³ The PS-*b*-P2VP-*b*-PNIPAM monoliths demonstrated an excellent stability over failure even at high feed pressure (over 2 bar) since a

linear change in water flux with the increase in pressure drop is observed regardless of the temperature (20°C and 46°C). Water permeance values were measured to be ~ 2 and $18 \text{ L.h}^{-1}.\text{m}^{-2}.\text{bar}^{-1}$ at 20°C and viscosity corrected at 46°C, respectively, which demonstrates the thermo-sensitive character of the PL-structured monoliths. Importantly, the flux performance recorded at 46°C was corrected for the temperature dependence of water viscosity to determine the temperature-dependent changes that only outcome from the thermo-responsive behavior of PNIPAM-based nanopores.^{7,12}

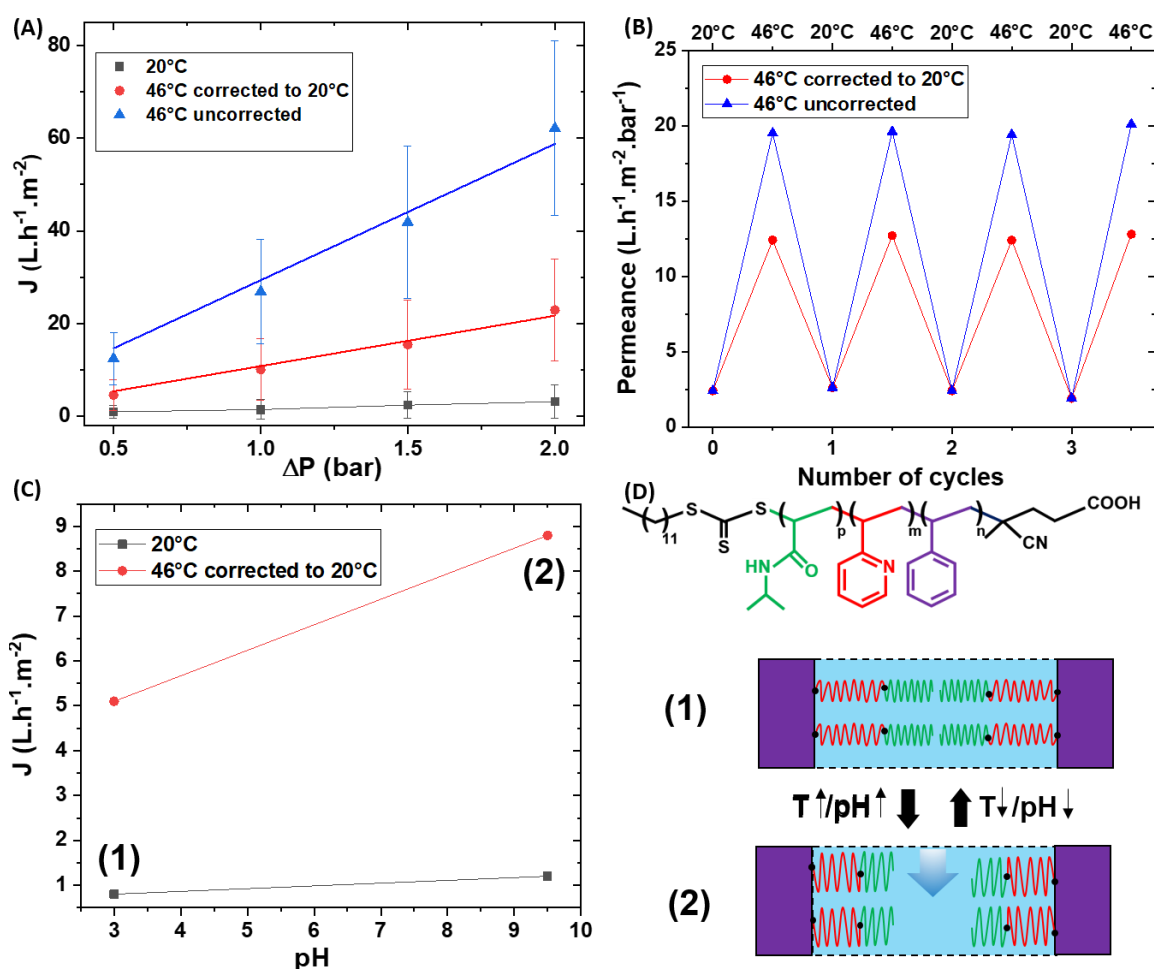


Figure 4. (a) Water fluxes, J , of the PS-*b*-P2VP-*b*-PNIPAM monoliths measured at different temperatures: (black squares) 20°C and viscosity corrected (red dots) 46°C. Uncorrected data (blue triangles) measured at 46°C are also given while error bars are the standard deviations of the mean relative permeance values calculated for two different samples. (b) Reversibility of the water permeance as a function of the temperature cycles (20°C and 46°C). Both uncorrected (blue triangles) and viscosity corrected (red dots) data are given. (c) J measured at 1 bar in acidic and basic water environments (pH = 3 and 9.5) for different temperatures: (black squares) 20°C and viscosity corrected (red dots) 46°C. (d) Schematic drawing of the PS-*b*-P2VP-*b*-PNIPAM terpolymer and illustration of the stimuli-responsive P2VP/PNIPAM nanopore behavior. The effective nanochannel porosity is regulated by the shape (*i.e.*, a swollen or shrunken state) of the P2VP and PNIPAM blocks according to changes of temperature and pH. (1) and (2) correspond to the close and open channel state, respectively.

Figure 4b shows a good temperature cyclability of the symmetric PS-*b*-P2VP-*b*-PNIPAM film between 20°C and 46°C. Indeed, at each cycle (*i.e.*, temperature switch), the permeance value matched with the previous one obtained at the same temperature. These results indicate that the well-defined PNIPAM-based nanochannels manufactured by NIPS-SVA have a fully reversible thermo-responsive character in accordance with a previous study reported by the Kamperman group on asymmetric single-responsive PS-*b*-PNIPAM membranes, however, endowed with short-range ordered nanopores.¹² Note also that the permeability values of these asymmetric single-responsive AB-type BCP membranes, measured above and below the PNIPAM LCST, are in the same range as those obtained in this work from symmetric dual-responsive ABC-type BCP membranes.

To go further in this study, the pH-sensitive character of the P2VP/PNIPAM nanoporous domains was also explored by measuring the viscosity corrected water fluxes under acidic and basic environments (at pH = 3 and 9.5) for two different temperatures (20°C and 46°C) (see **Fig. 4c**). The results revealed that the PS-*b*-P2VP-*b*-PNIPAM monolith generated by NIPS-SVA reaches various water flux values under the different conditions. This phenomenon occurs because the flux performance is closely related to the size of the adjustable porosity within the P2VP/PNIPAM nanochannels. The water channels are closed when the water flux test is conducted in an acidic environment (pH = 3) at 20°C (*i.e.*, below the PNIPAM LCST). This close channel state illustrated by the sketch (1) in **Figure 4d** corresponds to the case where both the PNIPAM and P2VP blocks are swollen, thereby leading to a small water flux value (0.8 L.h⁻¹.m² at 1 bar). Conversely, the highest water flux is achieved when the channel porosity is maximized by switching the pH environment to basic conditions (pH = 9.5) and increasing the temperature to 46°C (*i.e.*, above the PNIPAM LCST). This open channel state illustrated by the sketch (2) in **Figure 4d** corresponds to the case where both the PNIPAM and P2VP blocks are shrunken, which allows for a corrected water flux value of 8.8 L.h⁻¹.m² at 1 bar. Note that two partially open channel states can be reached when only one block shrinks within the P2VP/PNIPAM nanodomains. Therefore, an intermediate water flux value of 1.2 L.h⁻¹.m² at 1 bar is measured when only the P2VP block shrinks (pH = 9.3 and T = 20°C). Interestingly, the corrected water flux value (5.1 L.h⁻¹.m² at 1 bar) is substantially higher when only the PNIPAM block shrinks (pH = 3 and T = 46°C). This phenomenon could be attributed to the difference in size between the P2VP (5.8 kg/mol, $\phi_{P2VP} = 0.13$) and PNIPAM (8.5 kg/mol, $\phi_{PNIPAM} = 0.19$) blocks or could be due to the terpolymer chain architecture implying that P2VP and PNIPAM are the middle- and end-block, respectively, of the ABC-type BCP. In the last case, this makes

that the P2VP conformation changes under pH variations could be impeded by the absence of a free chain-end and/or could be due to a partial deprotonation of P2VP since the middle-block cannot be directly in contact with the water at basic pH.

Conclusion

In this study, a well-defined linear PS-*b*-P2VP-*b*-PNIPAM triblock terpolymer was synthesized for the first time by RAFT polymerization. The combination of the NIPS process with a SVA treatment was used to produce thermo/pH dual-responsive PL-structured PS-*b*-P2VP-*b*-PNIPAM monoliths with an adjustable nanochannel porosity. It is showed that the smart P2VP/PNIPAM nanochannels truly adopt an open or close state depending on the temperature and pH of water. An excellent temperature-reversible performance was also demonstrated by switching the water temperature below and above the PNIPAM LCST. These easy-to-clean nanostructured monoliths with thermo- and pH-responsive channels are envisioned to have potential in smart separation-based applications.

Experimental

Materials

N-isopropylacrylamide (NIPAM, >99%, Sigma-Aldrich) was purified by recrystallization in a mixture of toluene/hexane (50/50, v/v). Styrene (St, >98%, Sigma-Aldrich) was stirred with inhibitor removal resin about 30 min prior to use. 2-Vinylpyridine (2VP, >97%, Sigma-Aldrich) was passed through a column of activated alumina in order to remove the *tert*-butylcatechol present in the monomer. 2,2'-Azobis (2-methylpropionitrile) (AIBN, >99%, Sigma-Aldrich) was purified by recrystallization from methanol before being used. 4-Cyano-4-[(dodecylsulfanylthiocarbonyl)sulfanyl]pentanoic acid (CDPA, >97%, RAFT agent, Sigma-Aldrich) was used without further purification. All the solvents: 1,4-dioxane (DOX, >99%), tetrahydrofuran (THF, >99%), heptane, diethyl ether (>99%) and NMR solvents (*i.e.*, deuterated dichloromethane (CD₂Cl₂) and chloroform deuterated (CDCl₃)) were purchased from Sigma-Aldrich and used as received.

Synthesis procedures

Synthesis of the PS homopolymer macro-RAFT agent. In a typical experiment, a 100 mL round-bottomed flask was charged with 60 g of freshly purified styrene (0.57 mol), 0.26 g of CDPA (0.66 mmol) and 21 mg of AIBN (0.13 mmol). The sealed reaction vessel was purged with nitrogen and immersed in a preheated oil bath at 70 °C for 20h. The styrene bulk

polymerization was stopped by cooling the reaction vessel in an ice bath, then an aliquot was withdrawn from the solution to determine the monomer conversion by ^1H NMR. By comparing the integrated aliphatic proton signals due to the PS groups at 1.88 ppm to those due to the styrene monomer at 5.77–5.83 ppm, the conversion was found to be 39%. The resulting PS macro-chain transfer agent (CTA) was precipitated three times in cold methanol and dried overnight in a vacuum oven at RT) to give a white-yellowish powder. The molecular weight of hPS was determined solely by SEC since the CTA chain-end protons are not visible from the NMR spectrum. ^1H NMR (400MHz, CD_2Cl_2): $\delta = 6.59\text{--}7.05$ (5H, m, Ph), 1.2–1.83 (3H,m,CH-CH₂-). SEC in THF at 35°C using PS standard: the molecular weight (M_n) and dispersity (Đ) values were found to be of ~ 28.2 kg/mol and 1.09, respectively. 2D-DOSY-NMR (600MHz, CD_2Cl_2): $D = 8.31 \times 10^{-11} \text{ m}^2 \cdot \text{s}^{-1}$.

Synthesis of the PS-*b*-P2VP macro-RAFT agent. In 200 mL round flask, hPS_{28.2k} (5 g, 0.17 mmol) was mixed with 2VP (28.82 g, 0.27 mol), AIBN (5.8 mg, 0.035 mmol) and 1,4-dioxane (54.9 mL). The solution was purged with nitrogen and then heated to 70°C by using a temperature controlled oil bath. Polymerization was allowed to proceed during 7h prior to stopping the reaction by immersing the vessel into an ice bath. An aliquot was withdrawn from the solution, then the brown mixture was concentrated, precipitated in heptane and dried overnight under vacuum at RT (5.45 g, yield = 16 %). The PS-*b*-P2VP macro-RAFT agent conversion was calculated by ^1H NMR to be 10.2 %, by comparing the integrated aromatic proton signals of the P2VP ring at 8.25 ppm to those of the 2VP monomer at 8.53 ppm. ^1H NMR (400MHz, CD_2Cl_2): $\delta = 8.25$ (1H,m Ph), 6.61–7.06 (8H,m,Ph) and 1.27–2.30 (6H,m,CH-CH₂). The PS-*b*-P2VP molecular weight and its PS volume fraction were determined by ^1H NMR to be 34.6 kg/mol and 0.83, respectively. SEC in THF using PS standard: $M_n = 41.8$ kg/mol, $\text{Đ} = 1.14$. 2D-DOSY-NMR (600MHz, CD_2Cl_2): $D = 6.60 \times 10^{-11} \text{ m}^2 \cdot \text{s}^{-1}$.

Synthesis of the PS-*b*-P2VP-*b*-PNIPAM terpolymer. The PS-*b*-P2VP_{34.6k} macro-RAFT agent (4.5 g, 0.13 mmol), NIPAM (4.42 g, 0.03 mol) and AIBN (2.13 mg, 0.013 mmol) were dissolved in 23.4 mL of 1,4-dioxane. The solution was purged with nitrogen and then placed in preheated oil bath at 70°C for 5h. The polymerization was stopped by placing the reaction vessel into ice bath and an aliquot was afterwards withdrawn. 1,4-dioxane was removed with a rotary evaporator after which the PS-*b*-P2VP-*b*-PNIPAM chains were dissolved in a small amount of THF. The ABC triblock terpolymer was precipitated once from cold diethyl ether, in order to eliminate the unreacted NIPAM monomer, and heptane. To properly eliminate the undesired PNIPAM dead chains, a Soxhlet extraction was carried out with ethanol at 95°C for 96h. The PS-*b*-P2VP-*b*-PNIPAM terpolymer was then concentrated, precipitated in heptane and dried in

vacuum oven at room temperature (RT). The conversion was calculated by ^1H NMR to be 56%, by comparing the integrated proton signals of the PNIPAM groups at 3.99 ppm to those of the NIPAM monomer at 4.01-4.13 ppm. ^1H NMR (400MHz, CD_2Cl_2): $\delta = 3,99$ (1H, s, CH), 1.13 (6H,m,CH₃-). ^1H NMR spectrum revealed that PS-*b*-P2VP-*b*-PNIPAM chains consisted of PS (28.2 kg/mol, $\phi_{\text{PS}} = 0.68$), P2VP (5.8 kg/mol, $\phi_{\text{P2VP}} = 0.13$) and PNIPAM (8.5 kg/mol, $\phi_{\text{PNIPAM}} = 0.19$). SEC in THF using a PS standard revealed a M_n value of ~ 46.4 kg/mol ($\bar{D} = 1.32$) which is close to the one obtained by NMR (42.5 kg/mol). 2D-DOSY-NMR (600MHz, CD_2Cl_2): $D = 5.01 \times 10^{-11} \text{ m}^2 \cdot \text{s}^{-1}$.

Characterizations

^1H NMR and SEC characterizations. ^1H NMR spectroscopy were carried out on a Bruker Advance spectrometer operating either at 400 or 600 MHz using deuterated dichloromethane (CD_2Cl_2) or deuterated chloroform (CDCl_3). SEC was carried out on a Viscotek device (Malvern Instruments, Worcestershire, U.K) with a triple detector array. The SEC apparatus was equipped with two PLgel $5\mu\text{m}$ 500\AA columns, THF as eluent with a flow rate at 1mL/min at 35°C, PS standards were used for calibration of the column. Omniseq software using refractive index and light scattering signals was applied to calculate M_n and \bar{D} of polystyrene synthesized. M_n of all block copolymers were calculated using the M_n of their PS macro-RAFT agent obtained from SEC and the block ratios obtained from ^1H NMR results.

Fabrication of asymmetric PS-*b*-P2VP-*b*-PNIPAM thick films by NIPS: Freestanding 21 μm thick PS-*b*-P2VP-*b*-PNIPAM films were drawn onto (3 x 3 cm) silicon substrates by using a simple tape casting technique with 250 μm gap from a 18 % wt. terpolymer solution in a di-solvent mixture (DOX/THF: 1/1 by weight) (see **Fig. S10**). Solvents were allowed to evaporate during 30s at RT to form a dense air surface layer with a (kinetically trapped) poorly defined nanostructure, and then the PS-*b*-P2VP-*b*-NIPAM thick films were immersed into a deionized water bath at RT for 5 min to induce the polymer precipitation. In order to facilitate the removal of the terpolymer materials from the substrate, the silicon pieces were treated by an oxygen plasma in a home-made chamber (plasma conditions: 45 W, 75 mTorr O₂, 10min) prior to their use, then a sacrificial poly(3,4-ethylenedioxythiophene) polystyrene sulfonate (PEDOT:PSS) was inserted by spin-coating between the substrate and the PS-*b*-P2VP-*b*-PNIPAM thick films. It is noteworthy that the PS-*b*-P2VP-*b*-PNIPAM chains were solubilized in a large amount of THF (50 % wt.) in order to avoid their precipitation as observed in the commonly used DOX/THF: 4/1(by weight) mixture after several days.

Fabrication of the PL-structured PS-*b*-P2VP-*b*-PNIPAM monoliths by SVA: The self-assembly of PS-*b*-P2VP-*b*-PNIPAM chains formed within the NIPS-made thick films was

promoted by exposing films during 6h to a continuous stream of CHCl_3 vapor produced by bubbling nitrogen gas through the liquid solvent as described previously.^{24,25} This continuous flow system was used to control the CHCl_3 vapor pressure in the chamber by dilution with a separate N_2 stream so that a solvent vapor consisted of 32 sccm CHCl_3 vapor and 8 sccm N_2 (total 40 sccm). Note that the NIPS process was initially used to generate asymmetric terpolymer films after the SVA treatment.²³ However, a long SVA time (> 2h) was required to achieve well-defined nanopores on the material top surface, making that only symmetric terpolymer films entirely composed of the PL phase were finally considered in this work.

AFM, SEM and GISAXS characterizations: Atomic force microscopy (AFM Nano-Observer, CSInstruments) was used in tapping mode to characterize the surface morphology of PS-*b*-P2VP-*b*-PNIPAM thick films. Silicon cantilevers (PPP-NCH, Nanosensors) with a typical tip radius of ~5 nm were used. The resonance frequency of the cantilevers was about 235 kHz. Prior AFM measurements, PS-*b*-P2VP-*b*-PNIPAM thick films were treated with a fluorine based plasma in a home-made chamber to improve the AFM topographic image contrast (plasma conditions: 45 W, 75 mTorr CF_4 , and 90s). Scanning electron microscopy (SEM, Hitachi S-4800) was used at an accelerating voltage of 5 kV to acquire top view and cross-section images of both asymmetric thick films and monoliths formed by PS-*b*-P2VP-*b*-PNIPAM chains. GISAXS experiments were performed on the Dutch-Belgian Beamline (DUBBLE) at the European Synchrotron Radiation Facility (ESRF) station BM26B in Grenoble.²⁶ A monochromatic beam of 12 keV was set using a Si (111) double crystal monochromator. The sample (typical size of 150 mm²) was shone with the X-ray beam with an angle of incidence of 0.2°, which is above the critical angle of the polymer, ensuring full penetration of the X-ray beam in the material and hence, analyzing the full volume of the sample. The 2D scattering patterns were collected with a PILATUS3 S 1 M detector. The scattering vector and the sample to detector distance were calibrated using silver behenate as standard, obtaining a sample-to-detector distance of 7500 mm.

Water flux performances: The water permeability of the different PS-*b*-P2VP-*b*-PNIPAM thick films was measured in a 10 mL filtration cell (Amicon 8010 stirred cell) connected to a water reservoir and a compressed air line. The measurements were performed on 2.5cm diameter PS-*b*-P2VP-*b*-PNIPAM material discs supported by a high permeable hydrophilic PVDF material (water permeability of ~2900 L h⁻¹ m⁻² bar⁻¹)²³ at pressures between 0.5 and 2 bar. The mass of water passing through the stacked materials (permeate) was recorded using a connected balance at regular time intervals for 10 min. Water temperature was maintained at

20°C and heated up to 46°C using a stainless steel electronic baths. Correction for the temperature dependence of water viscosity was obtained by multiplying the flux results with the relative change in dynamic viscosity of water at 46°C compared to that of water at 20°C. Hydrochloric acid and sodium hydroxide solutions were used for filtration experiments in acidic and basic conditions (pH = 3 and 9.5), respectively.

Acknowledgements

This work was performed within the support of the ANR JCJC AFM_Ring project, grant ANR-18-CE09-00xx of the French Agence Nationale de la Recherche and through the project TAKCLE/AXE-Membrane du Futur/09-2020 founded by the Institut Européen des Membranes (IEM).

References

- (1) Peinemann, K. V.; Abetz, V.; Simon, P. F. W. Asymmetric Superstructure Formed in a Block Copolymer via Phase Separation. *Nat. Mater.* **2007**, *6* (12), 992–996. <https://doi.org/10.1038/nmat2038>.
- (2) Abetz, V. Isoporous Block Copolymer Membranes. *Macromol. Rapid Commun.* **2015**, *36* (1), 10–22. <https://doi.org/10.1002/marc.201400556>.
- (3) Nunes, S. P. Block Copolymer Membranes for Aqueous Solution Applications. *Macromolecules* **2016**, *49* (8), 2905–2916. <https://doi.org/10.1021/acs.macromol.5b02579>.
- (4) Zhang, Y.; Mulvenna, R. A.; Qu, S.; Boudouris, B. W.; Phillip, W. A. Block polymer membranes functionalized with nanoconfined polyelectrolyte brushes achieve sub-nanometer selectivity. *ACS Macro Lett.* **2017**, *6*, 726–732, DOI: 10.1021/acsmacrolett.7b00278.
- (5) Qiu, X.; Yu, H.; Karunakaran, M.; Pradeep, N.; Nunes, S. P.; Peinemann, K. V. Selective Separation of Similarly Sized Proteins with Tunable Nanoporous Block Copolymer Membranes. *ACS Nano* **2013**, *7* (1), 768–776. <https://doi.org/10.1021/nn305073e>.
- (6) Zhang, Y.; Sargent, J. L.; Boudouris, B. W.; Phillip, W. A. Nanoporous Membranes Generated from Self-Assembled Block Polymer Precursors: Quo Vadis? *J. Appl. Polym. Sci.* **2015**, *132* (21), n/a-n/a. <https://doi.org/10.1002/app.41683>.
- (7) Cetintas, M.; De Groot, J.; Hofman, A. H.; Van der Kooij, H. M.; Loos, K.; De Vos, W. M.; Kamperman, M. Free-standing thermo-responsive nanoporous membranes from high molecular weight PS-PNIPAM block copolymers synthesized via RAFT polymerization. *Polym. Chem.* **2017**, *8*, 2235–2243, DOI: 10.1039/C7PY00023E.

- (8) Liu, H.; Zhu, J.; Hao, L.; Jiang, Y.; van der Bruggen, B.; Sotito, A.; Gao, C.; Shen, J. Thermo- and pH-Responsive Graphene Oxide Membranes with Tunable Nanochannels for Water Gating and Permeability of Small Molecules. *J. Membr. Sci.* **2019**, *587*, 117163, DOI: 10.1016/j.memsci.2019.06.003.
- (9) Chu, L.-Y.; Li, Y.; Zhu, J.-H.; Chen, W.-M. Negatively thermoresponsive membranes with functional gates driven by zipper-type hydrogen-bonding interactions. *Angew. Chem., Int. Ed.* **2005**, *44*, 2124–2127, DOI: 10.1002/anie.200462687.
- (10) Zhang, K.; Feng, X.; Sui, X.; Hempenius, M. A.; Vancso, G. J. Breathing Pores on Command: Redox-Responsive Spongy Membranes from Poly(Ferrocenylsilane)S. *Angew. Chem., Int. Ed.* **2014**, *53* (50), 13789–13793.
- (11) Liu, H.; Liao, J.; Zhao, Y.; Sotito, A.; Zhu, J.; van der Bruggen, B.; Gao, C.; Shen, J. Bioinspired dual stimuli-responsive membranes with enhanced gating ratios and reversible performances for water gating. *J. Membr. Sci.* **2018**, *564*, 53–61, DOI: 10.1016/j.memsci.2018.07.013.
- (12) Mocan, M.; Wahdat, H.; van der Kooij, H. M.; de Vos, W. M.; Kamperman, M. Systematic variation of membrane casting parameters to control the structure of thermo-responsive isoporous membranes. *J. Membr. Sci.* **2018**, *548*, 502–509, DOI: 10.1016/j.memsci.2017.11.047.
- (13) Schacher, F.; Ulbricht, M.; Müller, A. H. E. Self-Supporting, Double Stimuli-Responsive Porous Membranes from Polystyrene-Block-poly(N,N-Dimethylaminoethyl Methacrylate) Diblock Copolymers. *Adv. Funct. Mater.* **2009**, *19* (7), 1040–1045. <https://doi.org/10.1002/adfm.200801457>.
- (14) Clodt, J. I.; Filiz, V.; Rangou, S.; Buhr, K.; Abetz, C.; Höche, D.; Hahn, J.; Jung, A.; Abetz, V. Double Stimuli-Responsive Isoporous Membranes via Post-Modification of Ph-Sensitive Self-Assembled Diblock Copolymer Membranes. *Adv. Funct. Mater.* **2013**, *23* (6), 731–738. <https://doi.org/10.1002/adfm.201202015>.
- (15) Zhang, Q.; Gu, Y.; Li, Y. M.; Beaucage, P. A.; Kao, T.; Wiesner, U. Dynamically Responsive Multifunctional Asymmetric Triblock Terpolymer Membranes with Intrinsic Binding Sites for Covalent Molecule Attachment. *Chem. Mater.* **2016**, *28* (11), 3870–3876, DOI: 10.1021/acs.chemmater.6b01044.
- (16) Algarni, F.; Musteata, V. E.; Falca, G.; Chisca, S.; Hadjichristidis, N.; Nunes, S. P. Thermo-Responsive Membranes from Blends of PVDF and PNIPAM-*b*-PVDF Block Copolymers with Linear and Star Architectures. *Macromolecules* **2021**, *54*, 10235, DOI: 10.1021/acs.macromol.1c01372
- (17) Jung, A.; Rangou, S.; Abetz, C.; Filiz, V.; Abetz, V. Structure Formation of Integral Asymmetric

Composite Membranes of Polystyrene-Block-Poly(2-Vinylpyridine) on a Nonwoven. *Macromol. Mater. Eng.* **2012**, 297 (8), 790– 798, DOI: 10.1002/mame.201100359.

- (18) Bivigou-Koumba, A. M.; Kristen, J.; Laschewsky, A.; Müller-Buschbaum, P.; Papadakis, C. M. Synthesis of Symmetrical Triblock Copolymers of Styrene and *N*-isopropylacrylamide Using Bifunctional Bis(trithiocarbonate)s as RAFT Agents. *Macromol. Chem. Phys.* **2009**, 210, 565– 578.
- (19) Stegelmeier, C.; Filiz, V.; Abetz, V.; Perlich, J.; Fery, A.; Ruckdeschel, P.; Rosenfeldt, S.; Förster, S. Topological Paths and Transient Morphologies during Formation of Mesoporous Block Copolymer Membranes. *Macromolecules* **2014**, 47 (16), 5566– 5577, DOI: 10.1021/ma5004908
- (20) Zhang, Z.; Rahman, M. M.; Abetz, C.; Abetz, V. High-performance asymmetric isoporous nanocomposite membranes with chemically-tailored amphiphilic nanochannels. *J. Mater. Chem. A* **2020**, 8, 9554– 9566, DOI: 10.1039/D0TA01023E.
- (21) Ji, N.; Tang, P.; Qiu, F.; Shi, A. C. Kinetic Pathways of Lamellae to Gyroid Transition in Weakly Segregated Diblock Copolymers *Macromolecules* **2015**, 48 (23) 8681– 8693 DOI: 10.1021/acs.macromol.5b02023.
- (22) Aissou, K.; Mumtaz, M.; Bouzit, H.; Pécastaings, G.; Portale, G.; Fleury, G.; Hadziioannou, G. Bicontinuous Network Nanostructure with Tunable Thickness Formed on Asymmetric Triblock Terpolymer Thick Films. *Macromolecules* **2019**, 4413– 4420, <https://doi.org/10.1021/acs.macromol.9b00572>.
- (23) Aissou, K.; Bouzit, H.; Krusch, F.; Méricq, J.-P.; Cot, D.; Masquelez, N.; Roualdes, S.; Quémener, D. Asymmetric Solvent-Annealed Triblock Terpolymer Thick Films Topped by a Hexagonal Perforated Lamellar Nanostructure. *Macromol. Rapid Commun.* **2021**, <https://doi.org/10.1002/marc.202100585>.
- (24) Gotrik, K. W.; Hannon, A. F.; Son, J. G.; Keller, B.; Alexander-Katz, A.; Ross, C. A. Morphology Control in Block Copolymer Films Using Mixed Solvent Vapors. *ACS Nano* **2012**, 6 (9), 8052–8059. <https://doi.org/10.1021/nn302641z>.
- (25) Aissou, K.; Mumtaz, M.; Demazy, N.; Pécastaings, G.; Fleury, G.; Hadziioannou, G. Periodic Bicontinuous Structures Formed on the Top Surface of Asymmetric Triblock Terpolymer Thick Films. *ACS Macro Lett.* **2019**, 8, 923– 930, DOI: 10.1021/acsmacrolett.9b00403.
- (26) Portale, G.; Hermida-Merino, D.; Bras, W. Polymer research and synchrotron radiation perspectives. *Eur. Polym. J.*, **2016**, 81, 415-432, 10.1016/j.eurpolymj.2016.04.015.